A Marker of Pointwise T-Wave Amplitude Variability: Evaluation on Simulated and Real ECG

Julia Ramírez[1,2], Michele Orini[3], Derek Tucker[4], Esther Pueyo[2,1] and Pablo Laguna[2,1]

[1] Biomedical Research Networking Center in Bioengineering, Biomaterials and Nanomedicine (CIBER-BBN), Zaragoza, Spain.
[2] Biomedical Signal Interpretation and Computational Simulation (BSICoS) group, Aragón Institute of Engineering Research (I3A), IIS Aragón, University of Zaragoza, Zaragoza, Spain.
[3] Institute of Cardiovascular Science, University College London, London, UK.
[4] Sandia National Laboratories, Albuquerque, NM, USA.

Abstract

Quantifying the variability between different T-waves can shade light into the analysis of ventricular repolarization liability. The variability present in the time-domain (warping) can corrupt the direct measurement of T-wave amplitude variability. Dynamic Time Warping (DTW) and a variation based on a square-root slope function (SRSF) transformation of the original T-waves have been proposed to remove the underlying time-domain warping. We compared the performance of both warping algorithms in removing induced time-domain variabilities to a simulated electrocardiogram (ECG) signal, we assessed the robustness against additive Laplacian noise of d_y and d_a, two markers of T-wave amplitude variability, after the time-domain warping has been removed, and we used d_a to measure the T-wave amplitude variability induced in real ECG during a Tilt test. Results confirmed that d_a is a robust marker of T-wave amplitude variability not related to time-domain underlying warping and demonstrated that d_a is affected by changes in the sympathetic activity produced by a tilt test.

1. Introduction

The T-wave on the electrocardiogram (ECG) reflects the spatio-temporal repolarization heterogeneity of the ventricular myocardium and its duration and morphology are commonly used to diagnose pathologies and assess risk of malignant arrhythmias [1]. Variabilities in such spatio-temporal repolarization heterogeneities are associated with increased arrhythmic risk [2], and this motivates the comparison of T-wave morphologies. However, a serious challenge arises when the T-waves are observed with flexibility or domain warping along the time domain. This warping may denote an inherent variability produced by repolarization heterogeneities or changes in heart rate that needs to be separated from the variability along the amplitude domain.

The most traditional algorithm of time-domain warping is the dynamic time warping (DTW) [3], which performs a sample-to-sample projection of one T-wave to a reference T-wave that aims at minimizing the Euclidean distance between both T-waves. DTW leads to a warping function that can be used to remove the time domain variability present in the original T-waves and, then, compute the Euclidean distance between the reference and the warped T-wave to calculate the genuine amplitude variability. Recently, a variation of DTW was proposed [4, 5] based on a mathematical representation of the signals, called the "square-root slope function" (SRSF), to improve alignment and provide fundamental mathematical equalities that lead to a formal development of the warping problem. Together with the warping cost function, they proposed d_y, the Euclidean distance of the difference between the SRSFs of the reference and the warped T-waves.

The objectives of this study are (1) to demonstrate that the warping algorithm based on SRSFs is more capable than DTW in removing time-domain variability, (2) to propose a new marker of T-wave amplitude variability, d_a, with higher robustness against additive Laplacian noise than d_y, (3) to assess whether d_a can be used to quantify the changes in T-wave amplitude produced by a Tilt test.

2. Methods

2.1. Warping Functions and Amplitude Variability Markers

Consider two T-waves, $\boldsymbol{f}^r(\boldsymbol{t}^r) = [f^r(t^r(1)), ..., f^r(t^r(N_r))]^T$ and $\boldsymbol{f}^s(\boldsymbol{t}^s) = [f^s(t^s(1)), ..., f^s(t^s(N_s))]^T$, where $\boldsymbol{t}^r = [t^r(1), ..., t^r(N_r)]^T$ and $\boldsymbol{t}^s = [t^s(1), ..., t^s(N_s)]^T$ and N_r

and N_s being the total duration of $\boldsymbol{t}^r$ and $\boldsymbol{t}^s$, respectively. We take $\boldsymbol{f}^r(\boldsymbol{t}^r)$ as the reference T-wave and $\boldsymbol{f}^s(\boldsymbol{t}^s)$ as the T-wave to be compared with respect to $\boldsymbol{f}^r(\boldsymbol{t}^r)$.

Let $\boldsymbol{\gamma}(\boldsymbol{t}^r)$ be the warping function that relates $\boldsymbol{t}^r$ and $\boldsymbol{t}^s$, such that the composition $\boldsymbol{f}^s(\boldsymbol{\gamma}(\boldsymbol{t}^r))$ denotes the re-parameterization or time domain warping of $\boldsymbol{f}^s(\boldsymbol{t}^s)$ using $\boldsymbol{\gamma}(\boldsymbol{t}^r)$, i.e. $\boldsymbol{f}^s(\boldsymbol{\gamma}(\boldsymbol{t}^r))$ represents the amplitude values of $\boldsymbol{f}^s(\boldsymbol{t}^s)$ if its temporal vector was $\boldsymbol{t}^r$. Then, the DTW algorithm finds the optimal warping function, $\boldsymbol{\gamma}^*_{\text{W}}(\boldsymbol{t}^r)$, as:

$$\boldsymbol{\gamma}^*_{\text{W}}\left(\boldsymbol{t}^r\right) = \underset{\boldsymbol{\gamma}(\boldsymbol{t}^r)}{\arg\min} \left(\left\| \boldsymbol{f}^r\left(\boldsymbol{t}^r\right) - \boldsymbol{f}^s\left(\boldsymbol{\gamma}\left(\boldsymbol{t}^r\right)\right) \right\| \right). \quad (1)$$

The SRSF of a T-wave $\boldsymbol{f}(\boldsymbol{t})$ is defined in the following form [4, 5]:

$$\boldsymbol{q}_f\left(\boldsymbol{t}\right) = \text{sign}\left(\dot{\boldsymbol{f}}\left(\boldsymbol{t}\right)\right)\sqrt{\left|\dot{\boldsymbol{f}}\left(\boldsymbol{t}\right)\right|} \quad (2)$$

If we warp a $\boldsymbol{f}(\boldsymbol{t})$ by $\boldsymbol{\gamma}(\boldsymbol{t})$, the SRSF of $[\boldsymbol{f} \circ \boldsymbol{\gamma}](\boldsymbol{t})$ is given by: $\boldsymbol{q}_f(\boldsymbol{\gamma}(\boldsymbol{t}))\sqrt{\dot{\boldsymbol{\gamma}}(\boldsymbol{t})}$. Now, the optimal warping function was proposed in [4, 5] as the function that minimizes the Euclidean distance of the difference between the SRSF of the original signals, obtaining a transformed warping function, denoted as $\boldsymbol{\gamma}^*_{\text{TW}}(\boldsymbol{t}^r)$:

$$\boldsymbol{\gamma}^*_{\text{TW}}\left(\boldsymbol{t}^r\right) = \underset{\boldsymbol{\gamma}(\boldsymbol{t}^r)}{\arg\min} \left(\left\| \boldsymbol{q}_{f^r}\left(\boldsymbol{t}^r\right) - \left(\boldsymbol{q}_{f^s}\left(\boldsymbol{\gamma}\left(\boldsymbol{t}^r\right)\right)\sqrt{\dot{\boldsymbol{\gamma}}(\boldsymbol{t}^r)}\right) \right\| \right). \quad (3)$$

We can define two markers of amplitude variability:

$$d_y = \left\| \boldsymbol{q}_{f^r}\left(\boldsymbol{t}^r\right) - \left(\boldsymbol{q}_{f^s}\left(\boldsymbol{\gamma}^*_{\text{TW}}\left(\boldsymbol{t}^r\right)\right)\sqrt{\dot{\boldsymbol{\gamma}}^*_{\text{TW}}\left(\boldsymbol{t}^r\right)}\right) \right\|, \quad (4)$$

$$d_a = \frac{\left\| \boldsymbol{f}^r\left(\boldsymbol{t}^r\right) - \boldsymbol{f}^s\left(\boldsymbol{\gamma}^*_{\text{TW}}\left(\boldsymbol{t}^r\right)\right) \right\|}{\left\| \boldsymbol{f}^r\left(\boldsymbol{t}^r\right) \right\|} \times 100. \quad (5)$$

2.2. Signal Preprocessing and T-wave selection

Preprocessing of the ECG signals included low-pass filtering at 40 Hz to remove electric and muscle noise but allow QRS detection, cubic splines interpolation for baseline wander removal and ectopic beats detection.

Principal Component Analysis was calculated lead-wise over the T-waves from the available leads to emphasize the T-wave energy, improve its delineation and enhance morphological differences [6].

Each T-wave from the first principal component was selected using the T-wave onset and T-wave offset delineation marks [7]. Then, each T-wave was further low-pass filtered at 20 Hz to remove the components that could potentially corrupt the T-wave shape.

2.3. Simulation Study

The accuracy of the different markers of T-wave amplitude variability, d_y and d_a, in detecting T-wave amplitude variations was assessed by simulating, under the presence of different levels of additive noise, controlled variations in the T-wave duration.

Let the T-wave from a reference noise-free cardiac beat, sampled at 1 kHz, be the reference T-wave, $\boldsymbol{f}^r[\boldsymbol{t}^r]$.

T-wave amplitude variability was modelled by multiplying the deviations from the iso-electric line of each T-wave i by a sinusoidal wave in the following way:

$$\boldsymbol{f}^s_i\left(\boldsymbol{t}^r\right) = \boldsymbol{f}^r\left(\boldsymbol{t}^r\right) \cdot \left(1 + 0.15 \cdot \sin\left(\frac{\pi\left(i-1\right)}{I-1}\right)\right), \quad i = 1, ..., I, \quad (6)$$

T-wave time domain modulation was introduced by modifying the temporal domain of $\boldsymbol{f}^r[\boldsymbol{t}^r]$ according to the following equation:

$$\boldsymbol{t}^s_i = t^r(1) + \left(t^r(N_r) - t^r(1)\right) \cdot \left(\frac{\boldsymbol{t}^r - t^r(1)}{t^r(N_r) - t^r(1)}\right)^{\alpha(i)}$$
$$\alpha(i) = \left(\frac{0.45(i-1)}{I-1} + 0.8\right), \quad i = 1, ..., I \quad (7)$$

where i is the heart beat, and I is the number of modulated beats. The i-th modulated cardiac beat was obtained by transforming $\boldsymbol{f}^r[\boldsymbol{t}^r]$ to $\boldsymbol{f}^s_i[\boldsymbol{t}^s_i]$. Then, a computer-generated ECG signal was obtained by concatenating the $I = 300$ modulated cardiac beats after the reference cardiac beat. This led to a 301-beat ECG signal. Then, this computer-generated ECG signal was preprocessed, detected and delineated, and the T-waves were delimited as explained in section 2.2. The reference $\boldsymbol{d}^r_a = [d^r_a(1), ..., d^r_a(I)]$ and $\boldsymbol{d}^r_y = [d^r_y(1), ..., d^r_y(I)]$ series were obtained by warping each $\boldsymbol{f}^s_i[\boldsymbol{t}^s_i]$ with $\boldsymbol{f}^r[\boldsymbol{t}^r]$, located in the first beat using eq. (3) and applying eqs. (4 and 5).

Then, zero mean Laplacian noise was iteratively added to the computer-generated ECG signal, such that the signal-to-noise ratio (SNR) was, in decibels (dB): $\text{SNR} = \{6, 12, ..., 36\}$. The estimated $\boldsymbol{d}^{\text{SNR}}_a = [d^{\text{SNR}}_a[1], ..., d^{\text{SNR}}_a[I]]$ and $\boldsymbol{d}^{\text{SNR}}_y = [d^{\text{SNR}}_y[1], ..., d^{\text{SNR}}_y[I]]$ series were obtained by comparing the T-waves from the noisy modulated ECG signal with noisy reference T-wave, located in the first beat. The estimation errors were, then, calculated as:

$$e_d\left(\text{SNR}\right) = \sqrt{\frac{\sum_{i=1}^{I}\left(d^{\text{SNR}}\left(i\right) - d^r\left(i\right)\right)^2}{\sum_{i=1}^{I}\left(d^r\left(i\right)\right)^2}} \times 100, \quad (8)$$

where $d = \{d_y, d_a\}$. The noise generation and relative error measurement steps were repeated 50 times in order to have robust relative error values.

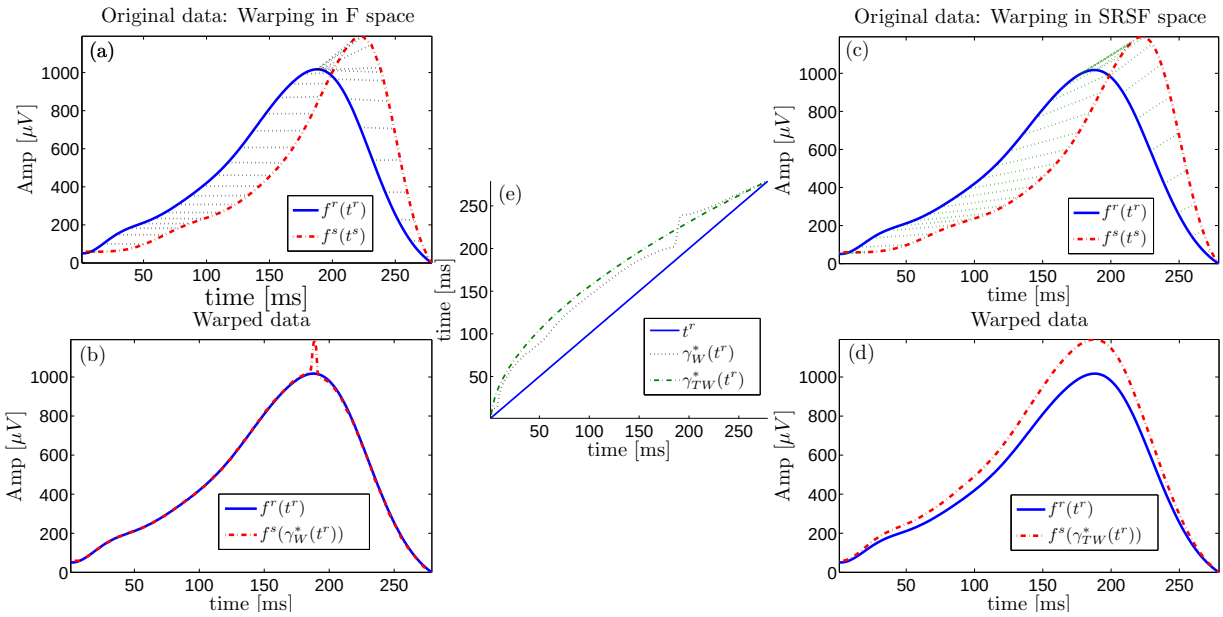

Figure 1. Demonstration of pinching problems using $\boldsymbol{\gamma}^*_{\text{W}}(\boldsymbol{t}^r)$ (left) and $\boldsymbol{\gamma}^*_{\text{TW}}(\boldsymbol{t}^r)$ (right).

2.4. Real ECG

ECG recordings from a database acquired at the University of Zaragoza for the study of the autonomic nervous system (ANS-UZ) were analyzed [8]. Recordings were obtained from 17 healthy subjects (age 28.5±2.8 years, 11 males) with no previous medical history related to cardiovascular diseases. Each recording consisted of 8 ECG leads, sampled at 1 KHz, acquired during a 13-min head-up tilt test (4-min supine, 5-min at 70°, 4-min supine).

The ECG recordings were preprocessed and delineated and d_a series were obtained for each subject by comparing each T-wave with the last one. The smoothed pseudo Wigner-Ville distribution (SPWVD) was used to estimate the time-varying spectral properties of d_a. The SPWVD of a signal $x(t)$ is defined as [9, 10]:

$$S_x(t,f) = \int\int_{-\infty}^{\infty} \kappa(\tau,\psi) A_x(\tau,\psi) e^{j2\pi(t\psi - f\tau)} d\psi d\tau \tag{9}$$

where $A_x(\tau,\psi)$ is the ambiguity function of $x(t)$, and $\kappa(\tau,\psi)$ is the elliptical exponential kernel defined in [11]. The range between 0.04 and 0.15 Hz (low-frequency component, LF) represents both sympathetic and parasympathetic modulation, although an increase in its power is generally associated with a sympathetic activation. The range between 0.15 and 0.4 Hz (high-frequency component, HF) corresponds to parasympathetic modulation and is synchronous with the respiratory rate. For each subject, the temporal evolution of the power content of d_a, within each frequency band, $P_B^{d_a}(t)$, were obtained integrating $S_x(t,f)$ in the frequency band B $\in$ {LF,HF}, respectively.

3. Results and discussion

3.1. Simulation Study

Figure 1 presents an example of warping functions using eq. (1) (left) and (3) (right). Top panels show $\boldsymbol{f}^r(\boldsymbol{t}^r)$ in solid blue and $\boldsymbol{f}^s(\boldsymbol{t}^s)$ in dash-dotted cyan. Bottom panels show $\boldsymbol{f}^r(\boldsymbol{t}^r)$ in solid blue and the warped $\boldsymbol{f}^s(\boldsymbol{t}^s)$ using either $\boldsymbol{\gamma}^*_{\text{W}}(\boldsymbol{t}^r)$ (left) or $\boldsymbol{\gamma}^*_{\text{TW}}(\boldsymbol{t}^r)$ (right). The fact that $\boldsymbol{f}^r(\boldsymbol{t}^r)$ and $\boldsymbol{f}^s(\boldsymbol{t}^s)$ have different amplitude values makes the cost function in eq. (1) to become degenerate and the resulting warped function to be "pinched". The cost function described in eq. (3), on the contrary, has a built-in regularization term, $\sqrt{\dot{\boldsymbol{\gamma}}^*_{\text{TW}}(\boldsymbol{t}^r)}$, that prevents it from becoming degenerate and resulting in absurd results. Therefore, we will only use $\boldsymbol{\gamma}^*_{\text{TW}}(\boldsymbol{t}^r)$ as the optimal warping function in the rest of this document.

Figure 2 shows the mean±standard deviation of the relative error between d_a^{SNR} and d_a^r (blue), and d_y^{SNR} and d_y^r (red), for different values of SNR. It can be seen how the relative error values of d_y are constantly higher than those from d_a. This is because d_y is calculated using the difference of the SRSFs of the original T-waves, and since the SRSF transformation is proportional to the derivative, it highlights the high components of the signal, but, at the same time, is less robust against additive broadband noise.

3.2. Real ECG

Since we have previously shown that d_a is not influenced by the "pinching effect", and is more robust against

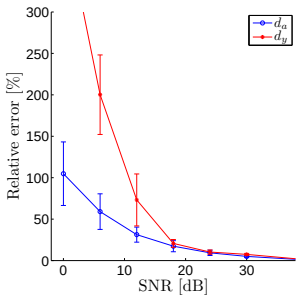

Figure 2. Relative error between reference and estimated d_a (blue) and d_y (red) under the presence of additive Laplacian noise.

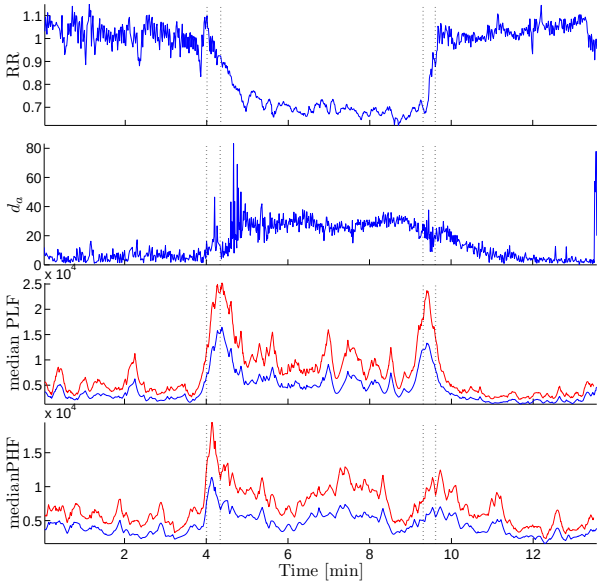

Figure 3. Temporal trend of the series during a Tilt test. (First and second panels) Temporal evolution of the RR and d_a series, respectively, for subject 9 in the database. (Thir and fourth panels): Temporal evolution of the instantaneous power of d_a in LF and HF, respectively, estimated as the median (blue) + median absolute deviation (red) among subjects.

additive Laplacian noise than d_y, we decided to use d_a to measure T-wave amplitude variability during a Tilt test.

The results of comparing the amplitude of each T-wave in the ECG- recording with the last one are reported in Figure 3. RR and d_a series for a subject (male, 24 years old) are shown in the top and second panels. The temporal evolution of the median (blue) + absolute deviation (red) instantaneous power in the LF and HF bands for d_a are reported in the third and fourth panels, respectively. The increase in $P_{LF}^{d_a}(t)$ during tilt indicates that d_a is affected by changes in the sympathetic activity, which have been shown to increase during orthostatic body positions [12].

4. Conclusions

The present paper proposes a novel marker of T-wave amplitude variability completely unrelated to non-linear time domain variability, robust against additive Laplacian noise and capable of quantifying the variability in the T-wave amplitude produced by an orthostatic change.

Acknowledgements

This work was supported in part by project TIN2013-41998-R from Spanish Ministry of Economy and Competitiveness (MINECO), Spain, and by Aragón Government, Spain and from European Social Fund (EU) through BSICoS group. The computation was performed at the High Performance computing platform of the NANBIOSIS ICTS, CIBER-BBN and I3A, Zaragoza, Spain.

References

[1] M. J. Burgess. "Relation of ventricular repolarization to electrocardiographic T wave-form and arrhythmia vulnerability." *Am J Physiol: Heart Circ Physiol* vol. 5, pp.H391–H402, 1979.

[2] M. Baumert, A. Porta, M. A. Vos, et al. "QT interval variability in body surface ECG: measurement, physiological basis, and clinical value: position statement and consensus guidance endorsed by the European Heart Rhythm Association jointly with the ESC Working Group on Cardiac Cellular Electrophysiology." *Europace* 2016; doi:10.1093/europace/euv405.

[3] T. K. Vintsyuk. "Speech discrimination by dynamic programming." *Cybernetics* vol. 4, pp.52–57, 1968.

[4] A. Srivastava, W. Wu, S. Kurtek, et al, "Registration of Functional Data Using Fisher-Rao metric", arXiv:1103.3817v2[math.ST], 2011.

[5] J. D. Tucker, W. Wu and A. Srivastava. "Generative models for functional data using phase and amplitude separation." *Computational Statistics and Data Analysis* vol. 61, pp. 50–66, 2013.

[6] F. Castells, P. Laguna, L. Sörnmo, et al. "Principal component analysis in ECG signal processing." *EURASIP Journal on Applied Signal Processing* vol. 2007, pp.98–119, 2007.

[7] J. P. Martínez, R. Almeida, S. Olmos, et al. "A wavelet-based ECG delineator: evaluation on standard databases." *IEEE Trans Biomed Eng* vol. 51, pp.570–581, 2004.

[8] A. Mincholé, E. Pueyo, P. Laguna. "Transmural differences in rate adaptation of repolarization duration quantified from ECG repolarization interval dynamics." *Computers in Cardiology* vol. 36, pp.597–600, 2009.

[9] F. Hlawatsch. "Duality and classification of bilinear time-frequency signal representations". *IEEE Trans Signal Process* vol. 39, pp.1564–1574, 1991.

[10] W. Martin, P. Flandrin. “Wigner-Ville spectral analysis of nonstationarity processes”. *IEEE Trans Acoust Speech Signal Process* vol. 33, pp.1461–1470, 1985.

[11] M. Orini, R. Bailón, L. T. Mainardi, et al. “Characterization of dynamic interactions between cardiovascular signals by time-frequency coherence.” *IEEE Trans Biomed Eng* vol. 59, pp.663–673, 2012.

[12] E. Gil, M. Orini, R. Bailón, et al. “Photoplethysmography pulse rate variability as a surrogate measurement of heart rate variability during non-stationary conditions.” *Physiol Meas* vol. 31, pp.1271–1290, 2010.

Address for correspondence:

Julia Ramírez
Campus Río Ebro, I+D Building, D-5.01.1B
Poeta mariano Esquillor, s/n
50018 Zaragoza (Spain)
Julia.Ramirez@unizar.es